Tr. J. of Physics
23 (1999) , 497 – 510.

Calibration of Millimetric Marmara Radio Telescope and Radio Detection of Ozone Line Over Gebze/Kocaeli in Turkey

M.E. ÖZEL, I.M. YUSIFOV, * A.O. ALLAKHVERDIEV, *
TUBITAK Marmara Research Centre,
PO Box 21, 41470, Gebze, Kocaeli-TURKEY
A.A. VERTIY,
TUBITAK-Marmara Research Center, Turkish-Ukrainian Joint Research Laboratory,
PO Box 21, 41470, Gebze, Kocaeli-TURKEY,
G. BAYER, O. DEMİRCAN,
Ankara Univ., Dept. of Astronomy,
Ankara-TURKEY,
H. KIRBIYIK, T. ADIGÜZEL,
Middle East Tech. Univ., Dept. of Physics,
Ankara-TURKEY,

Received 12.11.1997

Abstract

A brief description of the calibration procedures for the millimetric Marmara Radio Telescope, MRT-2 is presented. Observations carried out during the spectroscopic calibration work is indicative of daily variations of Ozone line of sight density over the telescope location. This being also the first radio observations carried out in Turkey, a short account of observations and results are given.

1. Introduction

2 m aperture Marmara Radio Telescope, MRT-2 (Fig. 1) sensitive to millimeter (mm) radio waves in the range of 85-115 GHz (3.5-2.6mm) has been installed in 1995 at Marmara Research Center (MRC) of the Scientific & Technical Research Council of Turkey, TUBITAK. The instrument was designed and built by the Institute of Radio

*On leave from Institute of Physics of Azerbaijan Academy of Sciences, 370143, Baku-AZERBAIJAN

Astronomy, Kharkov, Ukraine. Main goals of MRT-2 have been defined as the study of solar and planetary radiation, interstellar medium and galactic molecular spectroscopy. Remote sensing of Earth's atmosphere through spectroscopic monitoring of trace and greenhouse gases including ozone (O_3) has been added to this list recently.

MRT-2 has an alt-azimuth construction whose adjustment and calibration are proved to be a time consuming task [1]. After initial installment and orientation tests, a process for pointing and tracking accuracy assessment has been followed. The main beam size and shape have been determined by the standard procedures described below.

For the radiometric calibration of MRT-2, mapping and estimation of total fluxes from Sun and Moon at several frequencies were carried out [2]. For spectroscopic calibration, the ozone emission lines around 100GHz from the atmosphere is targeted and successfully detected. Due to popular and academic interest, an early publication of these results are warranted.

Figure 1. General view of MRT-2, 2m Marmara Radio Telescope, presently located at Gebze-Kocaeli, Turkey (longitude 29°26'50" E, latitude 40°47'13"N)

In this report, after a short description of MRT-2 calibration activites, we briefly review the atmospheric ozone problem and present the first radio measurements in Turkey, of ozone line emission via the same istrument.

2. Basic MRT-2 Instrumentation and its calibration

The MRT-2 antenna dish is a Cassegrain system with a parabolic reflector coupled to the total power receiving complex which consists of a diplexer, a mixer, a Phase-Locked

Loop (PLL) oscillator system and a low noise Intermediate Frequency (IF) amplifier. A diplexer couples the antenna input signal and the local oscillator voltage; feeds them into the double-side band (DSB) Ga-As Shottky-barrier mixer stabilized at room temperature. The mixer transfers the input signal into the first IF. As a local oscillator source, a backward-wave tube with a wide electrical tuning range is used. The operating frequency range of this system is tuneable between 85-115 GHz.

MRT-2 has two modes of operation: as a radiometer and as a spectrometer. In the radiometer regime, the output signal has a 400 MHz bandwidth and the total power of incoming radiation within this band is measured. In this mode, the signal passes through the first IF amplifier which is followed by the register/control system (the system computer). In the spectral mode, the central 16 MHz part of 400 MHz wide band signal goes into the first IF amplifier (with 1320 MHz central frequency), passes to the Prefilter Video/Converter (PVC) unit for the second step conversion down to the second IF (with a 16 MHz bandwidth around the central 40MHz frequency). The resultant useful signal is divided by an appropriate filter system into two equal channels, 8 MHz bandwidth each. These channel outputs are fed into the Digital Sign Correlator (DSC) which is used for the estimation of the normalized sign autocorrellation function of input signal. Fourier transform of input signal is used to obtain the power spectral distribution in the identical 8 MHz-bandwidth detectors which is split into 64 channels of 125kHz bandwidth/bin.

The measured main beam sizes of MRT-2 is quite close to its theoretical half power beam width (HPBW) with value of 5.9' at 90 GHz and 4.8' at 109 GHz (Fig. 2, Fig. 3 and [3]). However, the sidelobe levels are rather high by one order of magnitude over the expected. This is suspected to be due to the small but still significant off-axis alignment of the telescope optics causing some defocusing of the entire antenna system. Although this leads to some reduction in sensitivity, it does not cause significant obstacle for the observation of bright extended sources such as the Sun and the Moon and also the atmospheric ozone layer. Fine optical adjustment, which is critical for astrophysical faint and/or point source observations, is in progress.

The initial calibration of the receiver is performed by using, first, a hot black body (hBB) at ambient temperature at ∼290K and a cold black body (cBB) at liquid nitrogen temperature of 77 K. During the observation process, the atmospheric conditions as well as receiver parameters may sometimes change fast. Therefore, all 3 channels (400 MHz continuum and two 8 MHz spectral channels) are calibrated every 30 min by the hBB and cBB. The measured DSB receiver noise temperature T_n at the 400 K and for the two 8 MHz channels T_n were 495 K and 525 K, respectively.

Below we discuss the ozone layer observations carried out by MRT-2 during the winter of 1996-1997 after a short introduction to the atmospheric ozone problem.

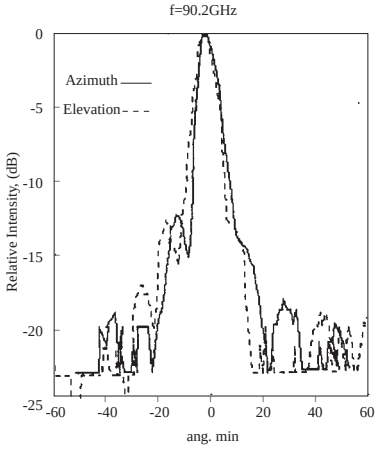

Figure 2. Antenna pattern of MRT-2 in azimuth and elevation, around $\mp$ 60' of pointing direction, at 90.2GHz

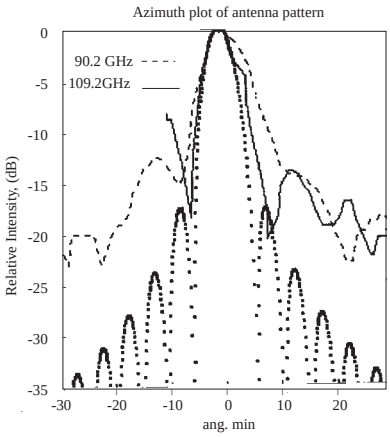

Figure 3. Measured antenna pattern of MRT-2 in two frequencies and its comparison with the normalized power pattern of $P_n(u) = \Lambda_1^2(\pi u D/\lambda)$ calculated for perfect reflecting surface, where $\Lambda_1(x) = 2J_1(x)/x$, $J_1(x)$ being the 1^{st} order Bessel function, and $u = sin(\theta)$, where θ is the angle from the axis of the central antenna beam. The theoretical pattern is drawn as dots for frequency 109.2 GHz.

3. Ground-based monitoring of ozonosphere in mm waves

By preventing the passage of intense solar ultraviolet (UV) radiation to the Earth's surface, the ozone layer plays an important role in the defense of the biosphere. However, the process is somewhat more complicated and requires further attention. Ozone absorbs not only UV, but also visible and infrared radiation causing considerable greenhouse effect. Through this process, changes in ozone concentration play an important role in the total radiation balance of the Earth's atmosphere and climate. Detection of total atmospheric ozone depletion over the poles [4] have created large excitement and interest in the ozone layer formation, its chemistry and depletion processes. Global investigations of distribution and variation of ozone layer over time and geographic position have accumulated much literature [5-7]. At present time, there are more than 70 ozone sounding/monitoring stations over the world [8].

Main methods of stratospheric ozone detection are the absorption of visible, ultraviolet and infrared radiation in the ozone lines by Dobson spectrometers [9]; the chemiluminissent methods; and direct measurements of ozone using balloons, aircrafts, rockets and satellites.

The results of ground-based detection of the tropospheric ozone concentrations car-

ried out over more than 100 years, are summmarized in [10]. Figure 4, adopted from [10], illustrates the evolution of the tropospheric ozone, since 1870 over Pic du Midi Observatory, France. An increase, amounting to 2.4 % per year over the last 20 years is visible over Western Europe.

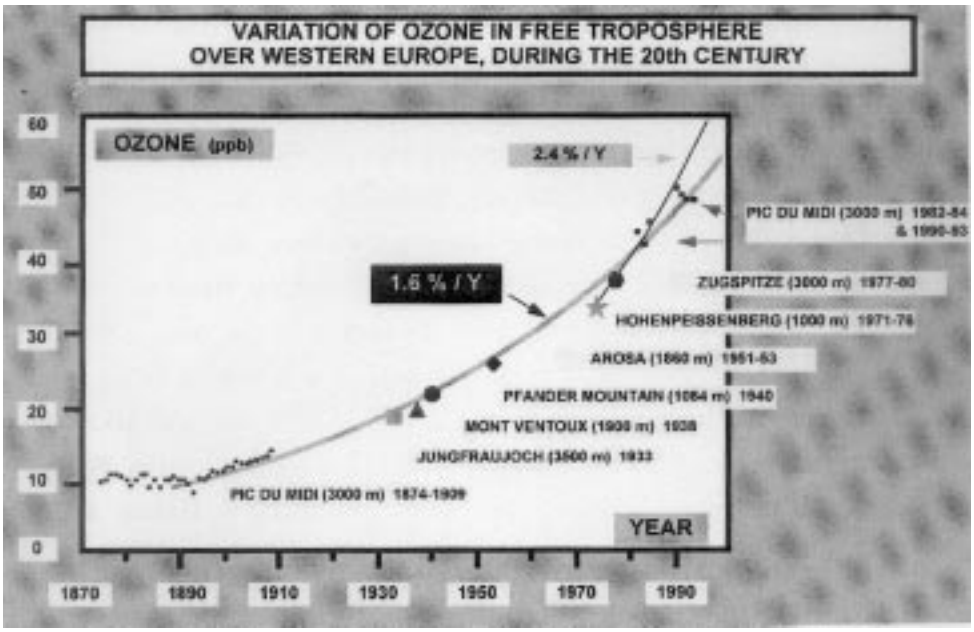

Figure 4. Ozone evolution in the lower atmosphere (in parts per billion scales-pbb-) over Western Europe from measurements at the Pic du Midi Observatory (France) and in various other European stations at high altitudes.

Other series of long period (1926 to 1996) ground-based total ozone measurements at Arosa (Switzerland) are available by Internet [11]. An increase of tropospherical ozone by a factor of two between 1950-1995 is also found by this data set. However, the total ozone concentrations obtained by the NIMBUS [12] satellite data show a clear decline during the last the years (Fig. 5)

The increase of tropospheric ozone did not and does not compensate the total ozone decrease [11], because only ∼10% of ozone is located in the troposphere (at a height of 0 to 10 km), whereas ∼90% of total ozone is distributed in the stratosphere (at heights between 10 to 50 km).

In spite of the fact that the tropospheric ozone is a small fraction of the total atmospheric ozone, it is also a subject of much current interest. Excess tropospheric ozone above some definite level, leads to negative health effects on humans, such as difficulties in breathing and excess coughing [13]. The limiting level for such 'short time health effects' are considered as 120 part per billion (ppb) by US health standard [13]. Long

term effects, which involve potential loss of life rather than mere irratations, would be far more costly. It was shown that [13] prolonged excess of the ozone level above 80-100 ppb also damages agricultural crops, especially cotton and soybeans. Estimates for the monetary loss from crop damages range from $1 to $2 billion per year in the USA [13].

It was also shown [14] that the global concentration of tropospheric ozone increases due to human activities. High levels of ozone concentrations occur in Europe and other industrialized countries. However, almost no information on tropospheric ozone levels and systematic monitoring is available for many countries, including Turkey. In the present report, we only address ozone line measurements and density estimations, which are mostly of stratospheric origin.

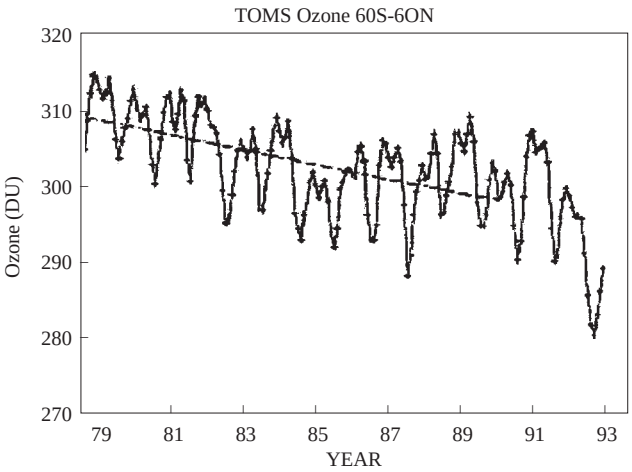

Figure 5. Monthly TOMS "global" ozone time series [12] from January 1979 through April 1993. For each month the area-weighted average from 60°S to 60°N is indicated by a +. The dashed straight line is the average trend for data through early 1990 (1 DU=$2.7\times10^{16} cm^{-2}$).

Complexity of the problem requires regular monitoring of the ozone. Recent development of mm-wave radio technology allows one to measure ozone's line of sight column density through the atmosphere. Ground-based ozone observations at milimetric waveband also have some distinct advantages over traditionalones in the optical (IR, visible and UV) range. We can record ozone lines day and night practically without any distortion, with relatively weak influence by weather and meteorological conditions and aerosols on the mm-wave propagation.

There are dozens of ozone lines in the 1,3 mm band, and the most intense are at 101.7; 110.8; 142.2 and 276.9 GHz. Measuring the profile of these lines with high resolution spectrometers allows one to calculate the vertical distribution of ozone through the well known inverse problem of spectral line formation. For its solution, the observed emission or absorption profiles of the ozone lines are used.

Absorption profiles can be obtained by measuring the optical depth of atmosphere, $\tau(\nu)$ around the ozone frequencies. In this method, the extinction of solar continuum emission or lunar radiation are measured at various zenith angles. In the literature, this is known as the 'Buger method' [15]. The method requires the presence of a strong extraterrestrial source of radiation, such as the Sun or the Moon.

Another detection method of ozone line profile is the measurement of atmospheric emission around the ozone line at a fixed latitude. By subtracting the background radiation we can obtain the targeted line profile. With MRT-2, it has been possible to successfully apply this technique. The present ozone measurements were carried out in the winter of 1996-1997, during the spectrometer calibration of MRT-2. The method of estimation of stratospheric ozone density profile and results obtained are given below.

4. MRT-2 observations of ozonosphere

Within the MRT-2 operating frequency band, the ozone molecule has 5 spectral lines at 96.2, 101.7, 103.9, 109.6, 110.8 GHz. For these lines the calculated average zenith brightness temperatures are 4.1, 7.7, 2.3, 2.5 and 12 K, respectively [16]. The most intense line is at the frequency ν_0=110.836 GHz. This line has a very wide shape [17] (about 600 MHz full width at zero level).

Scanning the available 400 MHz continuum window centered on frequency $\nu = \nu_0$ we carried out our ozone observations by using the two 8 MHz spectrometer channels as two independent radiometers tuned at different frequencies within this band. The wide band (400 MHz) radiometer was also used to estimate the atmospheric extinction around the ozone line.

The observations reported here were carried out at 3 different dates and times: 22 Nov. 1996 at 17^{00}-20^{00}UT, 31 Jan. 1997 at 11^{00}-14^{00}UT and 26 Feb.1997 at 11^{00}-15^{00}UT. On 26 Feb., observations of 2 bright ozone lines at 101.7 GHz and 110.8 GHz were carried out simultaneously. Due to very high level of noise at the line 101.7 GHz, the results from this line is not presently discussed here. During the first observing date on 22 Nov.1996, we carried our observations at different azimuth directions with constant elevation angle of 35^0 (or the zenith angle 65^0) at 4 different azimuth angle (A) directions from Gebze: 1) south (A=0^0, over Izmit Bay); 2) west (A=90^0, over the Marmara Sea); 3) north-east (A=125^0, over Istanbul) and 4) east (A=-80^0 over the city of Izmit). In spite of considerable different demographic and ecological conditions along searched directions (over the sea, land, a medium size city (Izmit) and a megalopolis (Istanbul)), we did not detect any significant differences among the observed total ozone line of sight intensities in these directions. For this reason, other observations were mainly carried out over the zenith and also to the south, in the directions of the Izmit Bay from MRC location, in Gebze.

To obtain the ozone line profile, the MRT-2 local oscillator needs to be manually adjusted to the required frequency, in this case around the ν_0=110.836 GHz line. The observations were carried out at frequency shifts of 0, 10, 25, 50, 75, 100, 150, 200 and 300 MHz from the central frequency of ozone line ν_0. For every frequency we have a pair of

outputs at $\nu_0 \mp 4$ MHz, corresponding to the centres of two 8MHz spectroscopic channels simultaneously. Every adjustment leads to a random shift of receiver noise temperature of about $\mp$ 5 K around the mean values ($\sim$440 K). The result is a rather noisy data. In order to reduce the spread of observational points, the running means of data points were calculated and the results are indicated by circles in Figures 6, 7, 8 for the 3 different dates mentioned. Indicated $\mp$5 K wide error bars in the figures are mainly a measure of uncertainties of random changes of noise temperature T_n due to the receiver, noted during the observations.

Due to high level of noise in the observing data, there were moments we were able to detect only one wing of the spectral line (Fig. 6 and Fig. 8). Spectral 'details' at the right sides of the main line (about 100 and 50 MHz from the line center) in the Figures 7 and 8 are most probably instrumental effects. In order to determine the nature of these details, further tests and observations are needed.

On the basis of these observations, we estimated the ozone number density profile in the stratosphere and checked our results against the US Standard Atmosphere models.

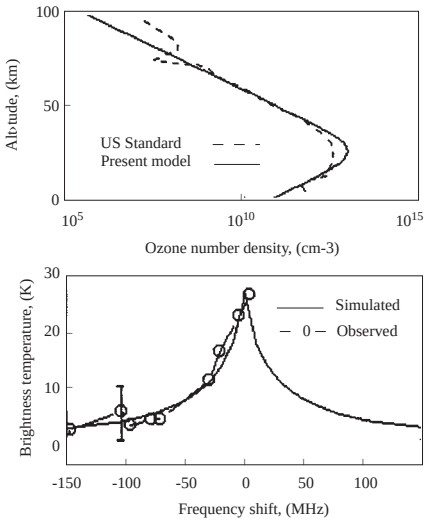

Figure 6. Ozone ν_0=110.836 GHz line observation over MRC-Gebze (Turkey), on 22 Nov. 1996 (17^{00}-20^{00}UT) at the zenith angel 65^{00}. In the lower part, the simulated ozone line profile (continuous line) is superimposed over the observed points (circles). In the upper part, the vertical distribution of ozone number density estimated in the present work is compared with the US Standard Atmospheric Model.

5. Estimation of the vertical distribution of ozone number density

In order to calculate the vertical atmospheric ozone profile we used the applicable radiative transfer equation [16] as:

$$T_A(\nu) = T_B(\nu)e^{-\tau} + \int_0^{\infty} T(h)exp(-\tau(h,\nu,T))k(h,\nu T)dh \qquad (1)$$

where $T_A(\nu)$ is the antenna temperature; $T_B(\nu)$ is the background temperature; τ is the atmospheric total opacity; T(h) is the atmospheric temperature height profile and $k(h,\nu,T)$ is the frequency-, altitude, and temperature- dependent atmospheric absorption coefficient in km^{-1} and h is the altitude, in km.

The background radiation $T_B(\nu)$ can be estimated from the off-line measurements by working at an equal zenith angle position. Absorption in the atmosphere arises mainly due to molecular oxygen (O_2) and water vapor [16,18] which are mainly concentrated below altitudes 8 km. However, ozone is distributed mainly at altitudes >8 km with maximum around 25 km. Neglecting the self absorption in ozone layer, which is an order of magnitude less than the water vapor absorption [16], Equation (1) can be rewritten as

$$T_A(\nu) = exp(-\frac{\tau}{cosz}) \int_8^{100} T_{0_3}(h).k(h,\nu,T)dh, \qquad (2)$$

where z is the zenith angle. The integration is carried out in the altitude limits of 8 to 100 km, where ozone is mainly distributed. τ, the atmospheric extinction, was determined before every observation by the 'antenna tipping' (skydip) method [19].

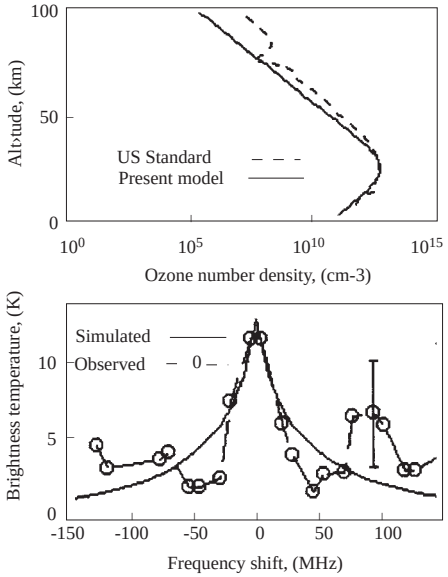

Figure 7. Ozone v_0=110.836 GHz observation on Jan.31,1997, (11^{00}-14^{00}UT) at the zenith angle 65°.

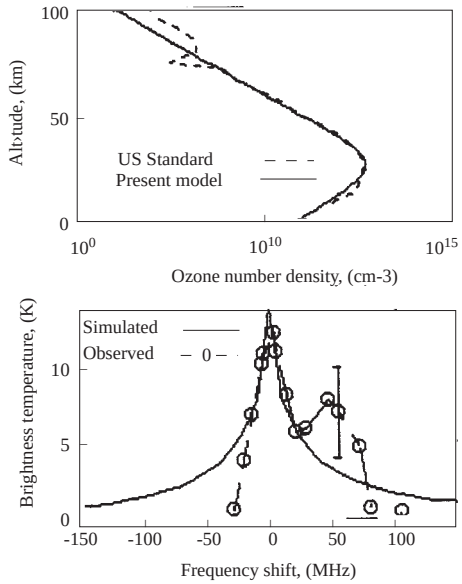

Figure 8. Ozone v_0=110.836 GHz observation on Feb.26,1997, (11^{00}-15^{00}UT) at the zenith angle 45°.

Absorption coefficient of ozone adopted from [20] has the form:

$$k = 1.7.10^{-24}\frac{exp(-25.3/T)}{T^{2.5}}Nv^2 f(\nu, \nu_0, \Delta\nu), \tag{3}$$

where k is in km^{-1}, T is the atmospheric temperature in K, ν is the operating frequency in Hz, N is the ozone number density in molecules cm^{-3}, ν_0=110.836×10^9 Hz, and $\Delta\nu$ is the constant line width in Hz. In our calculations we used the "kinetic line-shape" function [16,18]

$$f(\nu, \nu_0, \Delta\nu) = \frac{4\nu^2\Delta\nu}{(\nu^2 - \nu_0^2)^2 + 4\nu^2\Delta\nu^2}, \tag{4}$$

which is more correct in spectral line wings.

In the Earth's atmosphere up to 70km, collision broadening is more predominant than Doppler broadening. For this case, Doppler brodening may be neglected and as $\Delta\nu$ we used the empirical relation for collision (pressure) broadening [21]:

$$\Delta\nu = W\frac{P}{\sqrt{T}}, \tag{5}$$

where P is the atmospheric pressure in torrs (1 torr=1.33322 mB), W is a constant expressed in Hz K$^{1/2}$ torr^{-1} and is equal to 52.8×10^6 for the ambient temperature of 293 K. In our calculations as for the atmospheric pressure profiles, we considered the relation as in [22]:

$$P(h) = P_0 exp(-h/H), \tag{6}$$

where P_0=1013 mB, and pressure scale hight $H \cong 7$ km. As for the temperature profile of the atmosphere, we adopted the data from [23] for the proper time (season) and geographic latitude (see Fig.1) corresponding to the our observations.

The vertical distribution of ozone density may be approximated by various functions. For example, in [24] the ozone distribution is approximated by the simple exponential function, while in [25], by the sum of two exponential functions. For the present calculations of ozone density distribution, we chose the model of [25]:

$$N_{O_3}(h) = \frac{4D_m exp[r_m(h - h_m)]}{1 + exp[r_m(h - h_m)]^2} + D_p exp[-r_p^2(h - h_p)^2], \tag{7}$$

where D_m: density of the primary peak in the 15-30 km region (mol cm^{-3})

h_m : altitude of the primary peak (km)

r_m : shape factor (km^{-1})

D_p : density of the secondary peak located in the 60-90 km region (mol cm^{-3})
. h_p : altitude of the secondary peak (km)

r_p : shape factor (km^{-1}).

Second term ($D_p, h_p, r_p,$) in the right hand side of (7) arises due to nighttime enhancement of O_3 in the mesosphere [25]. The US Standard ozone density distribution, adapted from [16] and [26], is also shown in Figures 6, 7, 8 by dashed lines. The parameters of this distribution, obtained by fitting with the the Equation (7) are shown Table 1.

Varying these 6 parameters in the equation (7), we can find the best agreement between the observed and model ozone line profiles. In our models D_p, r_p, h_p are equal to zero, since we carried out our observations during daytime. (Corresponding parameters for the US Standard atmosphere are $1\times10^{-9}cm^{-3}, 0.2km^{-1}$ and 82 km).

Substituting the forementioned values of τ, T(h), P(h), $\Delta\nu$, N_{o_3} (h) and $k(h, \nu, T)$ into relation (2) and performing the integration with the indicated limits (8-100 km), we obtained the expected radiation profile of ozone line, which is superimposed with the observed profiles in the same Figures. The variable examined in these calculations is the ozone density profile N_{0_3} (h) of relation (3). As the ozone altitude profile, we selected the modeled distribution of N_{0_3} (h) that gives the simulated radiation profile the best matched the observed ozone emission line. As the criteria of agreement the simulated and observed line profiles, we considered the minimization of the function:

$$F(D_m, r_m, h_m, D_p, r_p, h_p) = \sum_{i=1}^{n} [T_0(\nu_i) - T_S(\nu_i, D_m, r_m, h_m, D_p, r_p, h_p)]^2, \qquad (8)$$

where n is the number of observed points in the line profile, ν_i is the radio frequency at which the observations of the given profile are made, $T_0(\nu_i)$ is the observed line profile and $T_s(\nu_i, D_m, r_m, h_m, D_p, r_p, h_p)$ is the simulated line profile calculated by using the relation (2).

With the minimizing of (8) for the parameters D_m, r_m, h_m, we have found the best coincidence of simulated and observed ozone line profiles. Then, using these parameters, by relation (7), we calculated the vertical distributions of ozone number density shown in Figures 6, 7, 8.

6. Results and Conclusion

The first scientific results from MRT-2 has been obtained during its spectrometer tests, by the first observation of the ozone line at ν_0=110.836 GHz over Gebze. This detection indicates that, the tuning precision of the high frequency tract of MRT-2 is no worse than a fraction of 8 MHz full bandwidth.

In general, the observed ozone line intensity at v=110836 MHz with the accuracy of the present (8MHz) spectrometer bandwith is in line with the expected values. This is also taken as an indicator of stability of the local oscillator and tuning precision of high frequency tract of MRT-2.

As for MRT-2 instrumentation and calibration process, telescope beam width is near the expected values except for higher side lobes, whose cause is attributed to slight

defocusing in optical alignment.

Our calculation results are presented in the Figures 6, 7, 8 in the form of vertical ozone density and corresponding radiated line profile. The best-fit model ozone line shapes are superimposed on the observed ozone line features (lower figures). Corresponding vertical distributions of ozone density are shown in the upper parts of every figure, together with the corresponding US Standard Atmospheric ozone distributions. Our results, are compared in Table 1 with the other parameters such as maximum ozone number density D_m and its corresponding altitude, h_m, of the US Standard Atmosphere altitude profile. The vertical column density of ozone in Dobson Units (DU) (1DU=$2.7\times10^{16}cm^{-2}$) found by the integration of ozone density given by (7), and is also given in the same Table. T_m is the brightness temperature at the ozone line center.

From the analysis of observational results we see that the observed ozone line brightness temperature is around the expected value of $T_{O_3} \cong$ 10-20 K [16,27]. The large deviation of estimated ozone column density on 22 Nov. 1996 is more probably connected with the errors due to random change of receiver noise temperature T_n and with the errors of due to baseline uncertainties.

Table 1. Comparison of MRT-2 Ozone observations at MRC-Gebze by the US Standard Atmosphere.

	$D_m^\star 10^{12}$ (cm^{-3})	h_m (km)	r_m (km^{-2})	T_m (K)	Total ozone (DU)
US Standard	5	24	0.22	10-20	323
22 Nov.1996 $17^{00}-20^{00}$UT	9	26	0.25	28∓5	527∓200
31 Jan.1997 $11^{00}-14^{00}$UT	4.4	24	0.25	12∓5	256∓50
26 Feb.1997 $11^{00}-15^{00}$UT	4	25.5	0.22	14∓5	260∓60

Present experience with the receiver complex of MRT-2 implies that to achieve more reliable temperature calibration levels, the receiver system need to be temperature calibrated to liquid nitrogen after every tuning of the local oscillator.

Further regular monitoring of the ozone observations with better frequency resolution will be very useful in understanding the spatial variation scale as well as the short and long term temporal variatons in the ozone content of the atmosphere. Regular daily observations of ozone from Gebze in the future[1] will allow us to investigate time behavior of ozone's vertical profile in more detail.

Acknowledgements

We thank Professors L.N. Litvinenko and V.M. Shulga, researchers and technicians

[1]PS: Due to mal function in MRT-2 receiver, such measurements are not carried out since 1997-August. The repair of the receiver is waited

Yu.V. Karelin, A.M. Korolev, V.I. Podyachii, E.A. Alexeev and V. Mishenko of RIAN Kharkov (Ukraina) for their help and guidence at various phases of telescope installation and calibration. We also thank Dr. S. Rasuloglu, H. Kaman, N. Pelitçi and R. Dermanlı for their participation in various procedures and actions along calibration and measurement phases. Our thanks are also due to Prof. A.G. Kislyakov from Nizhny Novgorod Univ. (Russia) for his valuable comments and helpful discussion, over the measurements and the text.

References

[1] Ulich, B.L., 1981, International J. of Infrared and Milimetre Waves, **2,** 293.

[2] M.E. Özel et al., 1997, in preparation .

[3] Özel, M.E., Yusifov, I.M., Karelin, Y., et al. 1996, X Astronomical Regional Conference University of Istanbul, 3-6 Sep. 1996, Istanbul, Turkey, in press

[4] Farman, J.C., Gardiner, B.G., & Shamklin, J.D., 1985, Nature, **315**, 207.

[5] Ricaud, P., Brillet, J., de La Noe, J., & Parisot, J.P., 1991, J. Geophys. Res. **96,** 18617.

[6] Wang W.-C. Isaksen, I.S.A. (eds), **Atmospheric Ozone as a Climate Gas,**, NATO ASI Series, No. **32,** Springer Verlag, 1995,

[7] Kislyakov A.G., Shkelev E.I., Sayelyev D.V., Vaks V.L. in **Current Problems of Radiophysics,** Russia, Nijni Novgorod, 1996, pp. 62-66. (in Russian)

[8] Mohnen, V.A., in **"Atmospheric Ozone as a Climate Gas",** Wang W. C., Isaksen I.S.A. (eds), NATO ASI Series, No.**32**, Springer, 1995, pp.321-342.

[9] Dobson, G.M.B., 1957, Ann. Int. Geophys. Year, **5**, 46-89.

[10] Marenco, A., Jonguires, I., Gouget, H, Ndlec, P., in **"Atmospheric Ozone as a Climate Gas"**, Wang W. C. Isaksen I.S.A. (eds), NATO ASI Series, No.**32**, Springer, 1995, p.305.

[11] Ozone data of Swiss Meteorological Institute, available at:
ftp://bach.ethz.ch/pub/anne/www/Arosayear.dat
ftp://bach.ethz.ch/pub/anne/www/Arosamonth.dat

[12] Stolarski, R.S., McPeters, R.D. Gleason, J.F., in **Atmospheric Ozone as a Climate Gas",** Wang W. C., Isaksen I.S.A. (eds), NATO ASI Series, No.**32,** Springer, 1995, p 396.

[13] Sillman, S., 1993, Ann. Rev. Energy of Environment., **18**, pp. 31-56.

[14] Volz, A., Kley, D., 1988, Nature, **332,** 240-242.

[15] Voronov, V.N., Demkin, V.M., Kulikov, Yu. Yu., 1968, Izv. Vis. Uch. Zaved, **29,** 1403 (in Russian).

[16] Waters, J.W., in **"Methods of Experimental Physics,** Vol. 12, Astrophysics, part B; Radio Telescopes, Ed. Meeks, M.L., New York, San Francisco & London, Academy Press, 1976, 280.

[17] Koistinen, OP., Walmu H.T., Risnen, A.V., et al. 1993, IEEE Transactions on Microwave Theory and Techniques, **41**, 2232.

[18] Kislyakov, A.G., Kulikov, Yu.Yu., Riskin, V.G., 1979, in **Spectroscopic Investigations of Cosmic and Atmospheric Radiation,** Russia, Gorkij (Nijni-Novgorod)-1979, pp.84-123, (in Russian)

[19] Rohfls, K., Wilson, T.L., 1996, **Tools of Radio astronomy,** 2^{nd} edition, Springer Verlag, pp. 195.

[20] Shimabukuro, F.I., Wilson, W.J., 1973, J. Geophys. Res., **28,** pp. 6136-6139.

[21] Walshaw, C.D., 1995 Proc. Phys. Soc. **168,** 530.

[22] Wallase, J.M., Hobbs, P.W., **Atmospheric Science,** Academic Press, Inc., San Diego, California, 1977, P.15.

[23] Houghton, J.T., 1977, **The Physics of Atmosphere,** Cambridge Univ. Press, p,175.

[24] Borisov, O.N., et al., 1992, Microwave Observations of Stratospheric Ozone in Arctic, Preprint No. **306**, Inst. of Applied Phys. RAS, Nijni-Novgord, (in Russian).

[25] Shimabakuro, F.I., Smith, P.I., Wilson, W.J., 1977, J. App. Meteorology, **16,** 929.

[26] U.S. Standard Atmosphere Supplements, 1966, US Printing Office, Washington, D.C., 1966.

[27] Sobel'man, I.I., Solomonov, S.V, Sorochenko, R.L., 1993, Vestnik Ross. Akad. Nauk., **63,** 721, (in Russian).